

Green synthesis of MIL-101(Cr) with enhanced direct air capture of CO₂ through synergistic effects of polyethyleneimine and additives

Kun Jiang ^a, Jian Yang ^{a,*}, Ximeng Liu ^a, Yao Tong ^a, Jichang Liu ^{b,*}, Jinlou Gu ^{a,*}

^a Key Laboratory for Ultrafine Materials of Ministry of Education, School of Materials Science and Engineering, East China University of Science and Technology, Shanghai 200237, China

^b School of Chemical Engineering, East China University of Science and Technology, Shanghai 200237, China



ARTICLE INFO

Keywords:

MOFs
Green synthesis
Amine functionalization
DAC
CO₂ capture

ABSTRACT

To address the continuously rising levels of CO₂ in the atmosphere and mitigate the greenhouse effect, CO₂ direct air capture (DAC) has become an increasingly important technology. Amines-functionalized metal-organic frameworks (MOFs) are promising to serve as adsorbents for CO₂ adsorption in DAC applications. This study presents a green synthesis approach for MIL-101(Cr) (MIL = Materials of Institut Lavoisier) using NaOH as a modulator, achieving a high specific surface area and uniform morphology while ensuring an eco-friendly process free from toxic chemicals and organic solvents at relatively low reaction temperature. Then, we explored the impact of co-impregnation of polyethyleneimine (PEI) and various additives (including hydroxyl-containing surfactants, alkanolamine and amine small molecules) into MIL-101(Cr) on the improvement of low concentration CO₂ adsorption at room temperature. The hydroxyl-containing surfactants not only provided hydroxyl groups to synergistically interact with amine sites for the DAC of CO₂, but also enhanced the dispersion of PEI within MIL-101(Cr) for the improved accessibility of the adsorption sites. As a result, the combination of PEI and polyethylene glycol (PEG) achieved the highest CO₂ adsorption capacity up to 1.65 mmol/g and amine efficiency of approximately 0.159 under 400 ppm CO₂ level. It also showed excellent adsorption kinetic performance and cyclic capacity. Breakthrough adsorption tests further validated the rapid and sustained removal of CO₂ with high selectivity under simulated dry and humid air environments, contributing to the development of more efficient adsorbents for DAC technology.

1. Introduction

The greenhouse effect from increasing greenhouse gas emission has become a critical challenge, with atmospheric CO₂ levels rising from around 300 ppm in 1830 to over 400 ppm in 2021, highlighting the urgency of addressing this issue [1–4]. While the development of clean energy can help reduce CO₂ emission, it cannot fully address the existing buildup of CO₂ in the atmosphere. Carbon capture and storage (CCS) technologies are essential for meeting low CO₂ emission standards and enabling the utilization of captured CO₂ in various settings, including industrial waste gas treatment, aviation, cold storage, and other confined spaces [5–10]. Among CCS methods, direct air capture (DAC) technology stands out as a promising negative emission technology, capable of capturing CO₂ directly from ambient air at very low levels [10–12]. However, DAC still faces significant challenges due to the low CO₂ concentration in the atmosphere (around 0.4 mbar), requiring

highly efficient adsorbents for selective capture of CO₂ from air [12–14].

Current DAC technologies mainly rely on liquid absorption or solid adsorption. Liquid absorption using amine-based solutions, such as monoethanolamine (MEA), affords high selectivity and capacity but frequently suffers from issues such as toxicity, volatility and high energy consumption during regeneration [8,11,15]. Solid adsorbents are more stable and easier to regenerate, but are limited by their relatively lower capacity, selectivity, and susceptibility in the presence of competitive adsorption by water vapor and other gases [16]. To overcome these restrictions, solid amine adsorbents have been developed, combining the advantages of high CO₂ adsorption capacity of liquid amines with the stability and ease of regeneration of solid adsorbents [17–23].

Metal-organic frameworks (MOFs) have emerged as one of the most promising adsorbents for the immobilization of solid amines due to their large surface areas, tunable structures as well as high stability [24–31]. Among various MOFs, MIL-101(Cr) has garnered particular attention

* Corresponding authors.

E-mail addresses: jianyang@ecust.edu.cn (J. Yang), liujc@ecust.edu.cn (J. Liu), jinlougu@ecust.edu.cn (J. Gu).

thanks to its exceptionally large surface area ($>3000 \text{ m}^2/\text{g}$) and chemical stability, making it an ideal candidate for CO_2 capture [32]. Extensive researches have demonstrated the potential of MIL-101(Cr) for CO_2 capture, and its adsorption capacity can be significantly enhanced through the functionalization with amine especially polyethylenimine (PEI) [33–37]. The high density of amine groups in PEI facilitates strong chemisorption of CO_2 , providing high selectivity and adsorption capacity even at low CO_2 concentrations. For example, Darunte et al. achieved a CO_2 adsorption capacity of 1.35 mmol/g using PEI-impregnated MIL-101(Cr) at 400 ppm CO_2 [34]. Zhong et al. utilized a double-solvent method to graft three small molecule amines onto MIL-101(Cr), significantly improving CO_2 adsorption capacity [36].

Despite these advancements, the practical application of MIL-101(Cr) in DAC still faces challenges related to its harsh synthesis conditions [38]. Traditional synthesis methods for MIL-101(Cr) involved the use of toxic reagents, such as hydrofluoric acid (HF), and required high temperatures (220 °C), raising concerns about environmental impact, safety, and large-scale production [32]. Several alternative synthesis approaches have been explored to reduce the environmental impact while improving scalability [39–44]. For instance, Bromberg achieved HF-free synthesis at 218 °C, and Adamu et al. lowered the synthesis temperature to 150 °C, albeit with a decrease in the surface area of the materials [39,43]. Recent advances in green synthesis of MIL-101(Cr) included the use of recycled polyethylene terephthalate (PET) as the H_2BDC source at 215 °C [45] and solvent-free mechanochemical routes at 220 °C [46]. While these methods reduce reliance on conventional solvents or reagents, they still require energy-intensive high-temperature conditions (>200 °C), limiting their scalability and industrial viability. Therefore, the development of eco-friendly and scalable synthesis methods for MIL-101(Cr) with high crystallinity and specific surface area remains a significant challenge for large-scale industrial applications [47–49].

On the other hand, the main challenge for MIL-101(Cr) adsorbents in DAC is enhancing their CO_2 adsorption capacity at its low concentration. While the impregnation methods of monoamine and polyamine molecules have improved adsorption capacity at low CO_2 partial pressures, the maximum amine loading in adsorbents is limited, restricting further improvements in adsorption capacity [34,37]. Moreover, excessive polyamine molecules would aggregate and cross-link, restricting the

accessibility of adsorption sites and reducing CO_2 adsorption capacity [50,51]. Previous studies have shown that adding hydroxyl (–OH) group containing additives can enhance both adsorption capacity and amine efficiency in CO_2 capture, which is typically evaluated by the amount of CO_2 adsorbed with per amine group [50–54]. The –OH can change the chemical bonding mechanism between CO_2 and polyamines, thereby enhancing CO_2 adsorption capacity [53]. Therefore, these studies inspire us to develop green synthesis methods for constructing Cr-based MOFs and explore the synergistic effect of various additives and PEI to improve CO_2 capture efficiency in DAC.

Herein, we propose a green and scalable aqueous synthesis method for MIL-101(Cr), using sodium hydroxide (NaOH) as the sole additive at a temperature of 130 °C, resulting in uniform spherical nanoparticles (NPs) with high crystallinity and surface area. Furthermore, we investigated the enhancement of CO_2 adsorption capacity by MIL-101(Cr) loaded with a combination of PEI and various additives. The hydroxyl-containing surfactants such as polyethylene glycol (PEG), Poly(ethylene oxide)-poly(propylene oxide)-poly(ethylene oxide) (P123), Polysorbate 20 (Tween20), the alkanolamines small molecules such as N-Methyl monoethanolamine (MMEA), diethanolamine (DEA), and 3-amino-1,2-propanediol (PPA) and, the small molecule amines such as diethylenetriamine (DETA), were co-impregnated with PEI into the MIL-101(Cr) adsorbent (Fig. 1). The results indicated that the hydroxyl-containing surfactants significantly enhanced both CO_2 adsorption capacity and amine efficiency under low CO_2 partial pressure. These functionalized materials demonstrate high adsorption capacity and selectivity under DAC conditions, underscoring their potential for more efficient CO_2 capture from the atmosphere.

2. Material and methods

2.1. Green synthesis of MIL-101 (Cr)

Initially, 4.00 g (10 mmol) of chromium nitrate nonahydrate ($\text{Cr}(\text{NO}_3)_3 \cdot 9\text{H}_2\text{O}$) was dissolved in 60 mL of deionized water, followed by the addition of 1.66 g (10 mmol) of 1,4-dicarboxybenzene (H_2BDC) and ultrasonic treatment for 10 min. Subsequently, 0.40 g (10 mmol) of NaOH was added and transferred to a 250 mL Duran bottle. The reaction was carried out at 130 °C for 48 h. The product was separated by

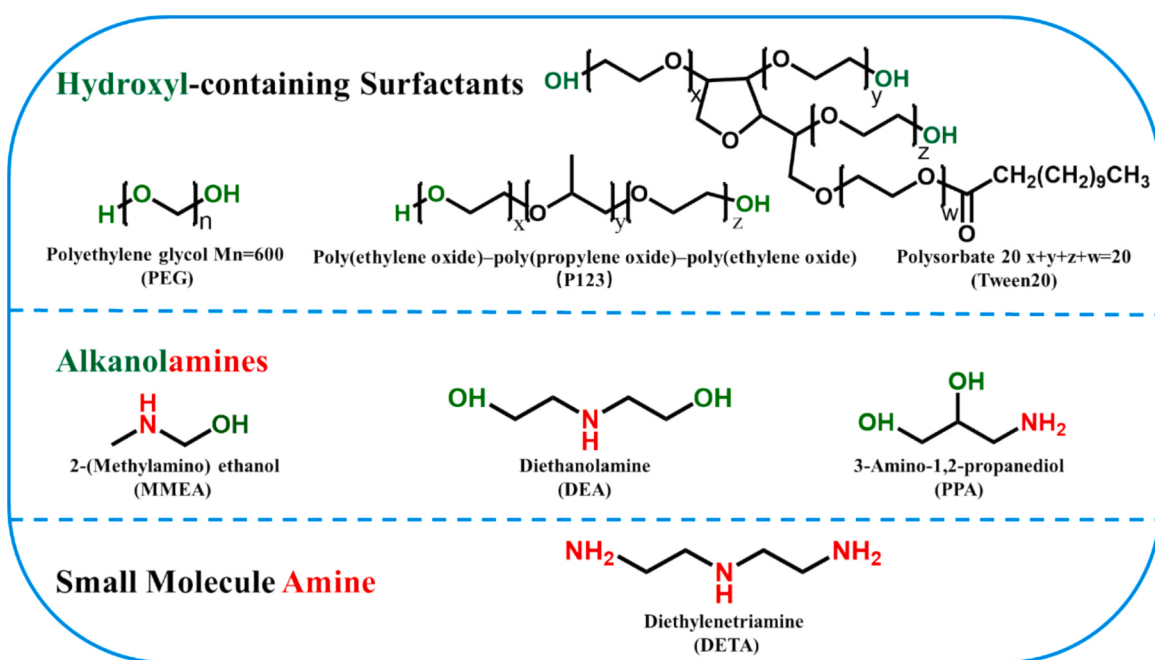


Fig. 1. The molecular formula of three types of additives applied to co-incorporate into MIL-101(Cr) with PEI in this work.

centrifugation (14,000 rpm, 10 min). The resulting solid was washed once with deionized water, twice with N, N-dimethylformamide (DMF) to remove unreacted H₂BDC, and then soaked in methanol for 24 h, with methanol replaced every 12 h. The solid was dried at 60 °C under vacuum. Before preparing the impregnated sample, MIL-101(Cr) was kept under vacuum conditions at 150 °C for 12 h.

Samples with different amount of NaOH (5, 7.5, 15 and 20 mmol) were synthesized in the same reactant conditions. Samples with different reaction times (24, 48 and 72 h) were synthesized in the same reactant ratio. Samples with different reaction temperatures (210, 200, 190, 180, 170, 160, 150 and 140 °C) were synthesized in the hydrothermal autoclave under the same conditions. The synthesis procedure using KOH as an additive was identical to that using NaOH, only replacing NaOH with KOH.

For the large-scale synthesis of MIL-101(Cr), a minor modification was made to the synthesis procedure. Initially, 40.0 g (0.1 mol) of (Cr (NO₃)₃·9H₂O) was dissolved in 500 mL of deionized water. This was followed by the addition of 16.6 g (0.1 mol) of H₂BDC, with the mixture then subject to ultrasonic treatment for 20 min. Subsequently, 4.0 g (0.1 mol) of NaOH was introduced, and the solution was transferred into a 500 mL Duran bottle. The reaction was conducted at 130 °C for 72 h. The remaining steps followed the same protocol as those for small-scale synthesis.

2.2. Co-impregnation of PEI and various additives into MIL-101(Cr)

The samples impregnated with both PEI and other additives were labeled as MIL-101-PEI-n-Additive-m, where 'n' and 'm' represented the respective percentages of PEI and additive based on the weight of the MIL-101(Cr). In a typical synthesis procedure, 100 mg of MIL-101(Cr) was added to 3 mL of methanol and sonicated for 20 min until a homogeneous suspension was formed. Meanwhile, 100 mg of PEI (branched PEI, Mw = 600) and 10 mg of additives (DETA, PEG, Tween20, P123, DEA, MMEA, PPA, and oleamidopropyl betaine (OAPB)) were dissolved in 1 mL of methanol and stirred for 15 min. The two solutions were then mixed and stirred at room temperature for 6 h. The resulting slurry was rotarly evaporated to remove the solvent, followed by vacuum drying at room temperature overnight.

2.3. CO₂ Isothermal adsorption experiment

CO₂ adsorption isotherms at 298 K and 0–1 bar were measured on a Micromeritics TriStar 3020 Plus. Before CO₂ adsorption, approximately 50 mg of powder sample was activated at 110 °C under vacuum for 3 h at the degassing station.

2.4. CO₂ temperature-programmed desorption (CO₂-TPD)

CO₂-TPD experiments were conducted on a Micromeritics Auto Chem II. Before adsorption, 50 mg of powder sample was activated at 110 °C and under vacuum for 3 h. Then, the sample was purged with helium gas at 110 °C for 1 h, and the adsorption experiment was initiated after cooling to room temperature. After adsorbing CO₂ on the powder adsorbent at room temperature for 2 h, helium gas was used for purging for 1 h to remove physically adsorbed CO₂, and then the temperature was increased at a rate of 10 °C/min up to 110 °C.

2.5. CO₂ adsorption-desorption kinetic and cyclic performance experiments

CO₂ adsorption kinetic experiments were conducted using a TGA system. Before adsorption, 10 mg sample was placed in an Al₂O₃ sample cell, heated to 110 °C, and maintained for 60 min under N₂ atmosphere to active the sample. During the adsorption process, mixed gas of CO₂/N₂ (0.04 % CO₂, 99.96 % N₂) was introduced for 120 min to adsorption. In the desorption phase, the temperature was rapidly increased to 110 °C

and maintained for 60 min to desorption.

Cyclic adsorption–desorption experiments were performed using the same instrumentation and followed a similar procedure. Between two cycles, the temperature was lowered to 25 °C and stabilized for 20 min before the next cycle.

2.6. CO₂ breakthrough adsorption

The breakthrough adsorption experimental setup for CO₂ adsorption studies is schematically shown in Fig. S1. In the experiment, approximately 0.5 g of sample was loaded into a quartz U-shaped adsorption bed. To prevent the leakage of the sample, both ends were sealed with absorbent cotton. The adsorption bed was then placed in a circulating water bath maintained at 25 °C to ensure constant temperature. The experiment utilized a mixed gas of CO₂/N₂ (0.04 % CO₂, 99.96 % N₂), and flow rate was set at 300 mL/min. The CO₂ concentrations downstream of the adsorption bed were continuously monitored using a CO₂ sensor (Dynament, accuracy of ±10 ppm), with readings recorded every 5 s. Meanwhile, the mass flow sensor (MF-4701, accuracy of ±(2.0 + 0.5 FS) %) read and recorded the gas flow rate every 5 s. The experiment continued until the downstream CO₂ concentration reached to 400 ppm.

In the experiments conducted under humid feed conditions, the humid gas was generated using a water bubbler. The gas passed through a 250 mL bubbler, which humidified it to approximately 100 % RH. Prior to initiating the adsorption, the mixture gas was continuously passed through the water bubbler for one hour to achieve gas–liquid equilibrium.

3. Results and discussion

3.1. Green synthesis and characterization of MIL-101(Cr)

The powder X-ray diffraction (PXRD) pattern of the MIL-101(Cr), synthesized at a lower temperature of 130 °C, exhibited diffraction peaks that match well with those of the simulated XRD (Fig. 2a). This result confirmed the successful green synthesis of highly crystalline MIL-101(Cr) with the additive of NaOH. The N₂ sorption isotherm presents the characteristic adsorption steps of the MIL-101(Cr) structure with abundant micropores and mesopores (Fig. 2b) [32]. The Brunauer–Emmett–Teller (BET) specific surface area of the material is approximately 3500 m²/g, surpassing those of most reported counterparts using other synthetic methods (Table 1). The nonlocal density functional theory (NLDFT) pore size distribution showed that the synthesized MIL-101(Cr) exhibited two mesopores at around 2.6 and 3.2 nm, which closely align with the theoretical cage sizes (Fig. S2). The observed hysteresis loop in the relative pressure range of 0.9–1.0 can be attributed to the accumulation pores between NPs. Although several synthesis methods can also achieve such Cr-based MOFs with high specific surface areas, these often required the use of highly corrosive additives such as HF or HNO₃, or involved the synthesis procedure at elevated temperatures (above 200 °C). In contrast, currently developed strategy enables the synthesis of MIL-101(Cr) with exceptionally high specific surface areas at lower temperatures without the need of organic solvents and toxic additives, which can be attributed to dual role of NaOH. Firstly, its addition increases the pH of the reaction system and facilitates the formation of Cr₃ clusters [55], which promotes the crystal nucleation. Second, OH[−] accelerate the deprotonation of H₂BDC ligands [42], facilitating their coordination with Cr₃ clusters to form MIL-101(Cr) crystals. This dual effect enables the low-temperature synthesis without the need for toxic additives such as HF.

Dynamic light scattering (DLS) analysis determined the average particle size of MIL-101(Cr) to be about 130 nm (Fig. 2c). Scanning electron microscope (SEM) and transmission electron microscopy (TEM) images further revealed that the material consisted of uniform spherical NPs with a size of approximately 120 nm (Fig. 2d and e), which slightly smaller than the size observed in DLS analysis. The addition of NaOH is

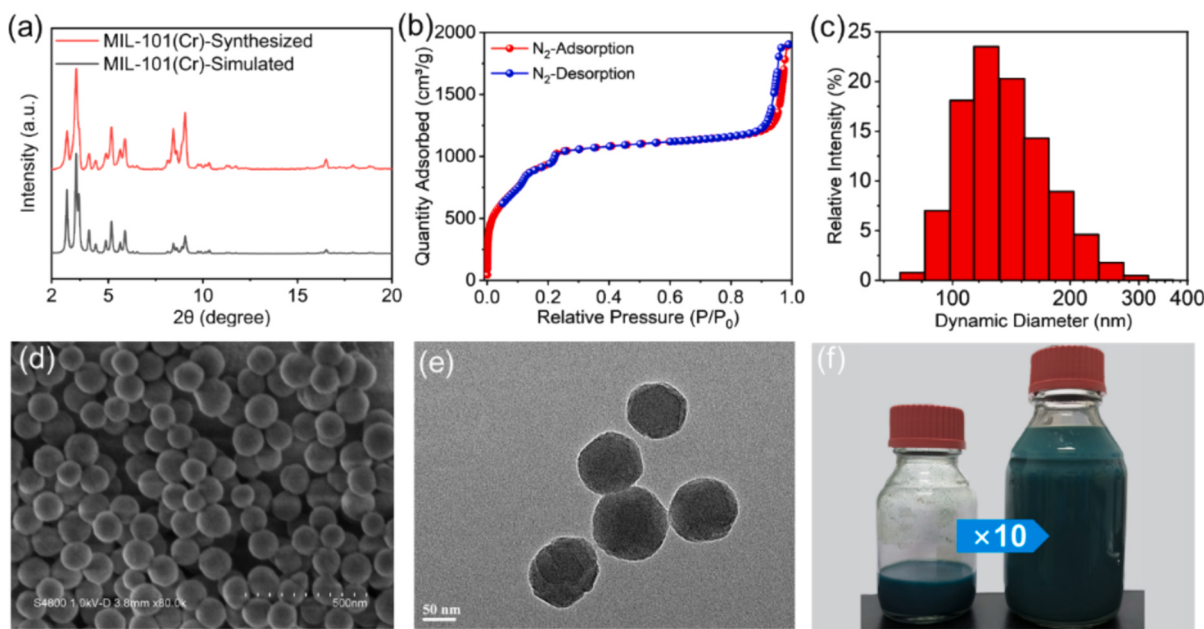


Fig. 2. (a) PXRD patterns of the as-synthesized and simulated MIL-101(Cr), (b) N_2 sorption isotherm of MIL-101(Cr), (c) DLS column graph of MIL-101(Cr) in an aqueous phase, (d) SEM and (e) TEM images of the as-synthesized MIL-101(Cr), and (f) the small and large-scale synthesis of MIL-101(Cr) based on the developed method.

Table 1

The comparison of the synthesis parameters for MIL-101(Cr) in this work and in the literatures.

Methods	Synthesis conditions			Textural properties		Refs.
	Medium	Temp. (°C)	Time (h)	BET specific surface area ($m^2 g^{-1}$)	Total pore volume ($cm^3 g^{-1}$)	
Hydrothermal	H ₂ O/NaOH	130	48	3529	1.89	This work
	H ₂ O/HF	220	8	4230	2.1	[32]
	H ₂ O	218	18	3460	N.A.	[39]
	H ₂ O	180	24	2250	1.24	[40]
	H ₂ O /HF	180	24	3184	1.53	
	H ₂ O/TMAOH	180	24	3197	1.73	
	H ₂ O/HNO ₃	220	8	3841	1.72	[41]
	H ₂ O	150	6	2592	1.09	[43]
	H ₂ O/HNO ₃	200	15	3450	1.66	[44]
	H ₂ O/HNO ₃	215	8	3431	1.68	[45]
Solvent-free	H ₂ O (PET was used as a source of linker)	215	8	1852	1.25	
	N.A.	220	4	/	/	[46]
Microwave	H ₂ O /HF	210	0.67	3900	2.3	[57]
Mixed-solvothermal	DMF/ H ₂ O	160	24	2453	1.16	[58]

crucial for the formation of smaller particles. The elevated pH increases the concentration of Cr₃ clusters and deprotonated ligands, which promotes nucleation and results in the formation of a large number of small crystals. The formation of the spherical morphology can be attributed to the low synthesis temperature. Higher reaction temperatures accelerate the dissociation and re-coordination of ligands and clusters, promoting crystal growth into larger dihedral octahedral shapes. In contrast, low-temperature synthesis slows down these processes, resulting in the formation of smaller spherical morphologies [56]. The relatively small size of MIL-101(Cr) NPs is beneficial for incorporating amines and additives into the mesoporous cages, while also reducing the diffusion resistance of CO₂ during adsorption. Furthermore, we scaled up the synthesis of sample by a factor of ten (Fig. 2f). Although some agglomeration was observed in the synthesized samples (Fig. S3), they maintained good crystallinity and high BET surface area (Figs. S4 and S5), demonstrating that this method is effective for scaling up the synthesis of MIL-101(Cr).

Our systematic optimization studies revealed that MIL-101(Cr) can be successfully synthesized across a broad temperature range of 130–210 °C using identical conditions, though crystallization failed to occur below the critical threshold of 120 °C. While all samples exhibited

N_2 sorption isotherm characteristics with mesopores and micropores in MIL-101(Cr) (Fig. S6), samples prepared at elevated temperatures exhibited progressively reduced specific surface areas (Table S1). Correspondingly, the PXRD patterns of the samples synthesized at higher temperatures demonstrated broader and weaker diffraction peaks, in line with the poorer crystallinity (Fig. S7). SEM images showed that the morphology of MIL-101(Cr) gradually transitioned from an octahedral shape to a well-defined spherical morphology as synthesis temperature decreased (Figs. S8 and 2d). These observations suggested that lower temperatures promoted a favorable balance between nucleation and growth in NaOH-assisted synthesis, enabling controlled crystal development.

Since 130 °C is the optimal reaction temperature, we further explored the effect of NaOH addition on the products at 130 °C. Increasing NaOH from 7.5 to 15 mmol resulted in smaller particles due to accelerated nucleation (Figs. S9 and S10). However, deviation from this concentration range (either higher or lower) resulted in either no product formation or amorphous materials. Notably, the maximum specific surface area was achieved at an optimal NaOH concentration of 10 mmol (Fig. S11). On the other hand, we observed that the particle

size increased from approximately 80 to about 200 nm as the reaction time was extended from 24 to 72 h under the reaction condition at 130 °C (Figs. S12–S14), further indicating the slow crystal growth process of MIL-101(Cr) in the proposed synthesis method. This increase in particle size was reflected by a corresponding rise in the peak intensity of the PXRD patterns (Fig. S15), indicating improved crystallinity. The crystallinity was significantly improved when the reaction time exceeded 48 h. The highest BET specific surface area was obtained at a reaction time of 48 h (Fig. S16). Therefore, these results confirmed the importance of optimizing both reaction temperature of 130 °C and reaction time of 48 h to achieve the best crystalline structure and specific surface area for MIL-101(Cr).

To demonstrate the applicability of using strong bases as additives, we conducted the MOFs synthesis using KOH instead of NaOH under otherwise the same conditions. The results showed that the samples synthesized with KOH also exhibited a spherical morphology (Fig. S17). The PXRD pattern of MIL-101(Cr) synthesized with KOH confirmed high crystallinity (Fig. S18), and the N₂ sorption curve closely matched with that of the samples synthesized with NaOH (Fig. S19). The specific surface area of the sample was calculated to be around 3199 m²/g. The successful synthesis of MIL-101(Cr) using KOH as an additive reinforces our strategy of employing various alkali bases to facilitate milder synthesis of Cr-based MOFs. Therefore, this approach not only broadens the selection of raw materials for industrial production but also enhances the flexibility of production strategies.

3.2. MIL-101(Cr) functionalization with various additives

PEI contains a high density of amine groups which provide strong chemical adsorption sites for CO₂, making it effective for capturing low concentrations of CO₂ in ambient air. In this study, PEI was used as the primary component, while surfactants, alkanolamines or small molecule amines were utilized as additives to incorporate with PEI into MIL-101(Cr) (Fig. 1), enhancing CO₂ adsorption capacity and amine efficiency through their synergistic effects.

Impregnation with PEI and various additives generally resulted in a reduction of XRD peak intensity compared to that of the original MIL-101(Cr) due to the weakened contrast between pore wall and pore channels (Fig. S20) [59]. Additionally, the diffraction peak at around 7.1° nearly disappeared, likely due to the complete occupation of the mesopores of MIL-101(Cr) by PEI and additives [52]. The N₂ sorption isotherms revealed a significant decrease in the BET specific surface area for the PEI-loaded sample compared to the original MIL-101(Cr) (Fig. S21), with the BET surface area dropping sharply from over 3500 to 414 m²/g. When PEG was combined with PEI for impregnation, the BET surface area further decreased to just 39 m²/g (Table S2). This result suggested that PEI and PEG could be co-impregnated into the mesopores of MIL-101(Cr), leading to the extensive filling of the pores and a substantial reduction in surface area. A similar trend was observed for the samples co-impregnated PEI with other additives, and the comprehensive data on the specific surface area and pore size for all samples was provided in Table S2. Notably, the BET specific surface area showed a more pronounced reduction as the molecular weight of the

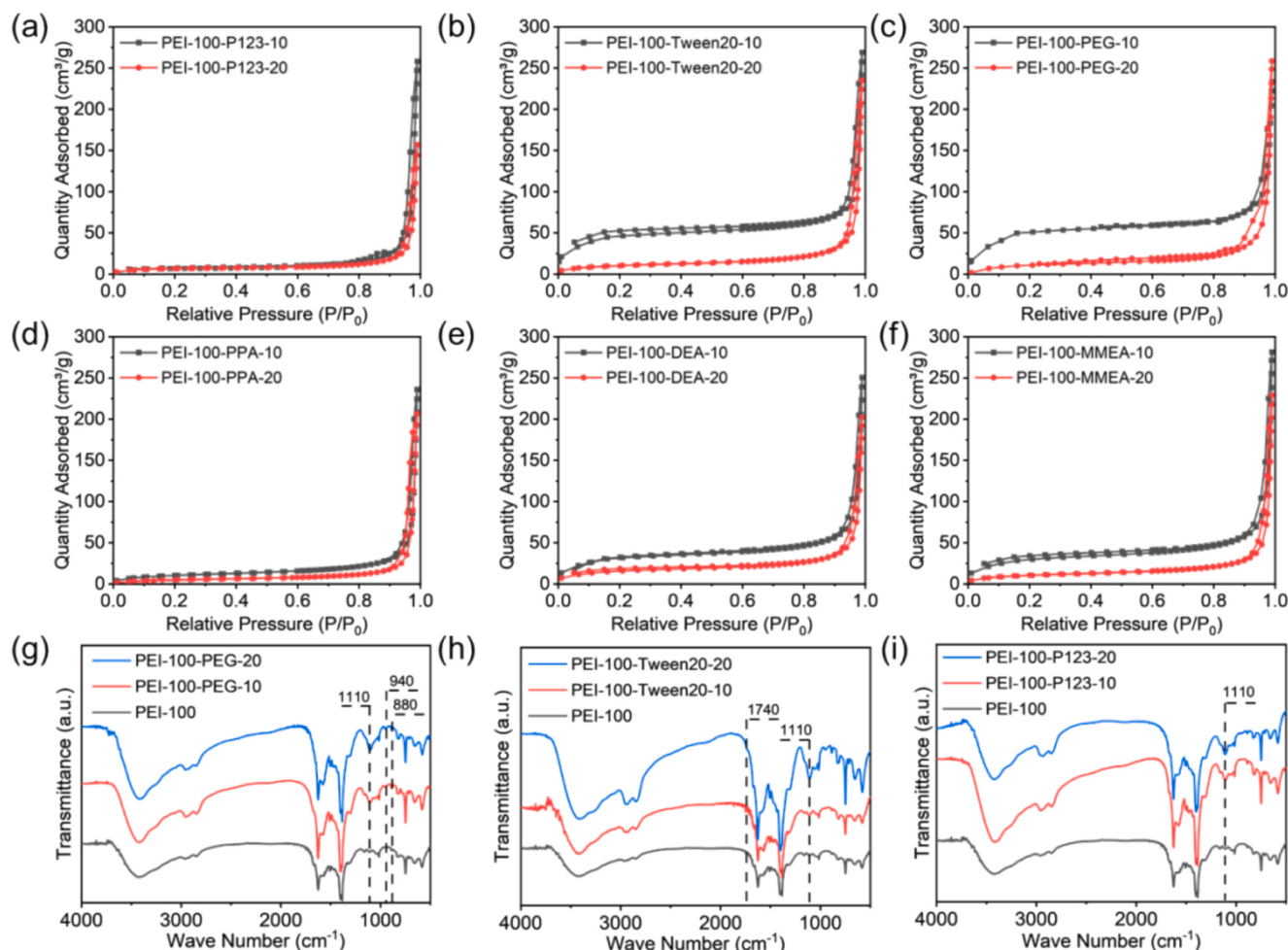


Fig. 3. N₂ sorption isotherms of the as-synthesized MIL-101(Cr) co-impregnated with PEI and (a) P123, (b) Tween20, (c) PEG, (d) PPA, (e) DEA, and (f) MMEA at 77 K. FT-IR curves of the MIL-101(Cr) co-impregnated with PEI and (g) PEG, (h) Tween20, and (i) P123.

additives increased, with P123 ($M_w = 5800$) > Tween20 ($M_w = 1228$) > PEG ($M_w = 600$) (Fig. 3a–c). Samples impregnated with three alkanolamines, OAPB and DETA additives also exhibited a decline in N_2 adsorption capacity, with the decrease being more significant as the quantity of the additive increased (Figs. 3d–f, S22 and S23).

The successful loading of the additives was further verified through FT-IR analysis. The band at around 1407 cm^{-1} in both the original and impregnated samples corresponded to the O–C–O vibration (Fig. S24), which was associated with the dicarboxylate group of ligands in the structure of MIL-101(Cr) [60]. Compared to the original sample, MIL-101(Cr)-PEI-100 displayed IR bands associated with methylene groups ($-\text{CH}_2-$) at 2950 and 2850 cm^{-1} , a peak at 1045 cm^{-1} corresponding to C–N, and a peak at 3248 cm^{-1} corresponding to amines groups ($-\text{NH}_2$) [59], confirming the successful introduction of PEI. The sample impregnated with both PEI and PEG exhibited a broad IR band at 1110 cm^{-1} (Fig. 3g), characteristic of the ethylene oxide (EO) fragment in PEG [61], thus confirming the successful introduction of PEG into the sample. Similar broad peaks at around 1110 cm^{-1} were observed in samples impregnated with P123 and Tween20 (Fig. 3h and i), corresponding to the characteristic peaks of PEO fragments in P123 and Tween20 [62]. Meanwhile, the samples impregnated with Tween20 displayed a distinct small band at 1740 cm^{-1} , associated with the carbonyl group ($\text{R}-\text{CO}-\text{O}-\text{R}$) of Tween20. These results confirmed that various hydroxyl-containing surfactant additives were successfully incorporated into MIL-101(Cr). Samples treated with alkanolamine additives (including MMEA, DEA, and PPA) exhibited enhanced amine-related IR bands at 3248 cm^{-1} (Figs. S25–S27), indicating an increased amine groups were introduced [59]. Additionally, these samples displayed enhanced hydroxyl-related bands at 1100 cm^{-1} , with the PPA-treated samples showing the most significant enhancement, attributed to the higher hydroxyl content of PPA. Samples treated with the small molecular amine of DETA exhibited enhancement exclusively in the amine-related bands (Fig. S28). Similarly, no noticeable enhancement was observed at 1110 cm^{-1} in samples treated with OAPB, attributed to the absence of hydroxyl groups (Fig. S29). Finally, nearly all samples containing additives exhibited intensified bands at 2950 and 2850 cm^{-1} , corresponding to methyl and methylene groups, respectively. These enhanced signals further confirmed the introduction of a large amount of additives into MIL-101(Cr).

Elemental analysis (EA) of the samples impregnated with PEI and various additives was shown in Table S3. The small amount of N element in the original MIL-101(Cr) sample was attributed to residual DMF remaining from the activation process. The addition of PEI into MIL-101(Cr) gave rise to a significant increase in nitrogen content. Upon co-impregnating PEI with alkanolamine and small molecule amine additives (such as MMEA, DEA, PAA, and DETA) into MIL-101(Cr), a further increase in nitrogen content was observed compared to the PEI-loaded sample. This increase can be attributed to the introduction of nitrogen-rich components of the alkanolamine and small molecule amine additives. However, the samples co-impregnated with PEI and hydroxyl-containing surfactants, such as PEG, Tween 20, and P123, exhibited only minimal changes in nitrogen content. This could be explained by the dual role of these surfactants. They enhanced the dispersibility of PEI, facilitating its penetration into the pores of MIL-101(Cr) and thereby slightly increasing the amount of PEI. However, since these surfactants lack nitrogen, the overall nitrogen content did not show an obvious increase.

3.3. CO_2 adsorption and amine efficiency of various functionalized MIL-101(Cr)

The CO_2 adsorption capacity and amine efficiency were evaluated at 298 K and CO_2 partial pressure of 400 ppm (Table S4). Under this condition, parent MIL-101(Cr) exhibited a negligible CO_2 adsorption capacity of 0.002 mmol/g (Fig. S30). In contrast, the MIL-101(Cr)-PEI-100 demonstrated a CO_2 adsorption capacity of 1.05 mmol/g and an

amine efficiency of 0.095 . Upon co-impregnation with small molecule amine of DETA, the CO_2 adsorption isotherm showed an improvement compared to that of the PEI-only sample (Figs. 4a and S31). The CO_2 adsorption capacity increased by nearly 32% (Fig. 4d), likely due to the higher amine loading introduced by DETA. However, the amine efficiency did not show a significant improvement. This indicated that although the addition of DETA increased the amine content, it did not enhance the accessibility of the chemical adsorption sites.

Next, we investigated the use of hydroxyl-containing surfactants (PEG, Tween20, and P123) as additives to enhance CO_2 adsorption capacity and amine efficiency when they were co-impregnated with PEI into MIL-101(Cr). The CO_2 adsorption experiments revealed that all hydroxyl-containing surfactants could significantly improve CO_2 adsorption under low-pressure conditions (Figs. 4b and S32). Among these, the sample with 20% PEG exhibited the best performance, achieving approximately 57% and 67% enhancements in CO_2 adsorption capacity and amine efficiency compared to the sample impregnated with PEI alone. Specifically, the CO_2 adsorption capacity and amine efficiency of MIL-101(Cr)-PEI-100-PEG-20 reached approximately 1.65 mmol/g and 0.159 at 400 ppm CO_2 (Fig. 4d), which exceed most reported MOFs-based adsorbents (Table S5). On the other hand, the performance of hydroxyl-containing additives was ranked as PEG > Tween20 > P123. This ranking correlates with the density of hydroxyl groups in each surfactant, with PEG exhibiting the highest concentration of hydroxyl groups per unit mass, followed by Tween20 and P123. This trend demonstrated that additives with a higher density of hydroxyl groups were competent to enhance the CO_2 adsorption capacity of PEI@MIL-101(Cr).

The dispersion effect of surfactants also played a crucial role in improving the dispersibility of PEI and enhancing its CO_2 adsorption performance. To demonstrate this, we selected OAPB, a surfactant without hydroxyl groups, and co-impregnated it with PEI into MIL-101(Cr). These samples still enhanced CO_2 adsorption capacity and amine efficiency, with an adsorption capacity of 1.53 mmol/g and an amine efficiency of 0.129 for MIL-101(Cr)-PEI-100-OAPB-10 (Figs. S33 and S34). This supports the view that effective dispersion of PEI within porous structures is crucial for improving CO_2 capture performance.

Finally, we also evaluated the effect of alkanolamine additives, including MMEA, DEA, and PPA on CO_2 adsorption. Compared to the hydroxyl-containing surfactants, these additives exhibited less promising performance (Figs. 4c and S35). Among the alkanolamine additives, the sample with 10% MMEA showed a 33% improvement in CO_2 adsorption capacity (1.40 mmol/g) and a 24% improvement in amine efficiency (0.118) compared to MIL-101(Cr)-PEI-100 (Fig. 4d). The sample with 10% DEA showed a moderate improvement, with a 15% increase in adsorption capacity (1.21 mmol/g) but only a negligible improvement in amine efficiency. Moreover, the sample with 10% PPA exhibited a 5% increase in adsorption capacity, accompanied by a slight decrease in amine efficiency. Despite containing both hydroxyl and amine groups, alkanolamines failed to outperform the performance of hydroxyl-containing surfactants. This phenomenon is primarily due to their inability to enhance the dispersibility of PEI within the MIL-101(Cr) cages as effectively as surfactants. Consequently, increasing the feed amount of alkanolamine additives to 20% led to a significant decrease in CO_2 adsorption capacity and amine efficiency, due to the reduced dispersibility of PEI and limited accessibility of adsorption sites.

We systematically investigated the relationship between PEI loading, additive loading, and adsorption performance using PEG as a representative additive. MIL-101(Cr)-PEI-100-PEG-25 and MIL-101(Cr)-PEI-100-PEG-30 exhibited adsorption capacities of 1.66 and 0.95 mmol/g , respectively (Fig. S36). Further elevation of PEG dosage to 30% paradoxically reduced adsorption capacity. Compared to the MIL-101(Cr)-PEI-100-PEG-20, the sample with the addition of 25% PEG showed an improvement of less than 1% . When the PEG loading was further increased to 30% , the adsorption capacity began to decrease. Although higher PEG loading can enhance the dispersion of PEI and increase the

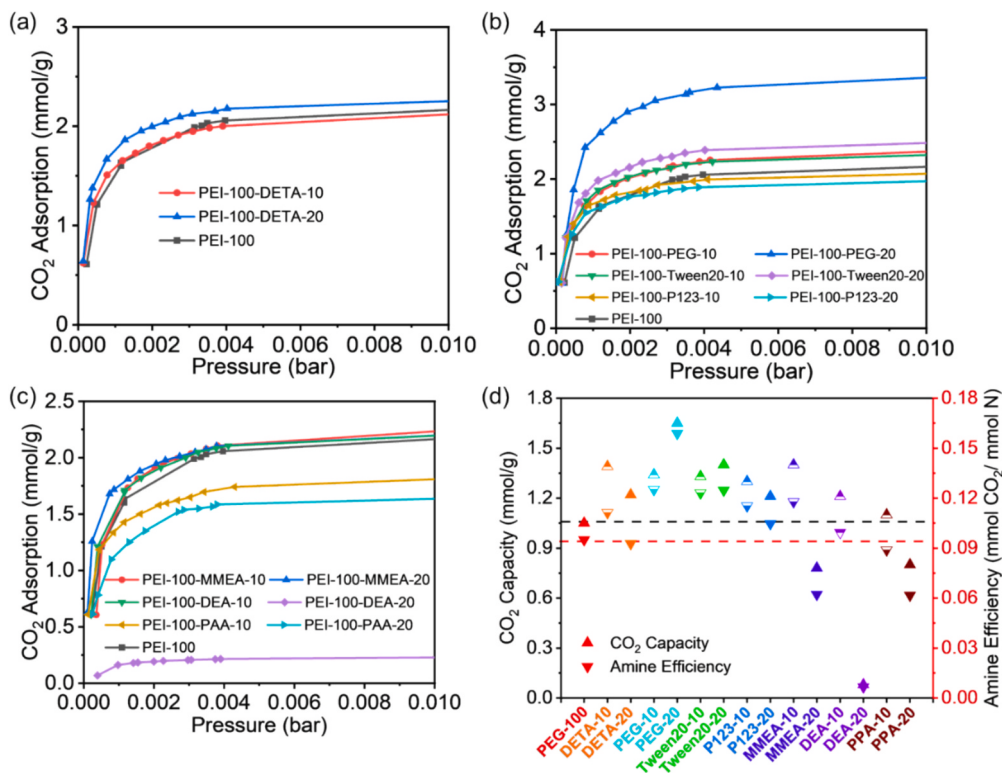


Fig. 4. CO₂ adsorption isotherms of MIL-101(Cr) co-impregnated with PEI and (a) DETA, (b) PEG, Tween20, P123, (c) MMEA, DEA and PPA between 0 to 0.01 bar. (d) The comparison of CO₂ adsorption capacities and amine efficiencies of various functionalized MIL-101 (Cr) at CO₂ partial pressure of 400 ppm.

availability of –OH sites, excessive PEG can adversely affect the pore structure by overfilling the pores. Notably, the efficacy of PEG in enhancing CO₂ adsorption capacity would be affected by PEI loading in MIL-101 (Cr). With 80 % PEI addition, the addition of 20 % PEG slightly increased the CO₂ adsorption capacity by 33 % in comparison to the MIL-101(Cr)-PEI-80 sample (Fig. S37). In contrast, the addition of 20 % PEG at MIL-101(Cr)-PEI-100 and MIL-101(Cr)-PEI-120 samples resulted in 57 % and 54 % improvement of the adsorption capacity, respectively.

For MIL-101(Cr)-PEI-120, severe aggregation caused the CO₂ adsorption isotherm to remain nearly unchanged after 0.0004 bar, indicating that most amine sites were ineffective for CO₂ adsorption. The addition of 20 % PEG into MIL-101(Cr)-PEI-120 significantly improved its adsorption performance (Fig. S38). This indicated that the addition of PEG had a positive effect on the CO₂ adsorption performance of all samples containing PEI. Moreover, the enhancement was more pronounced in samples with higher PEI loadings because higher PEI content caused

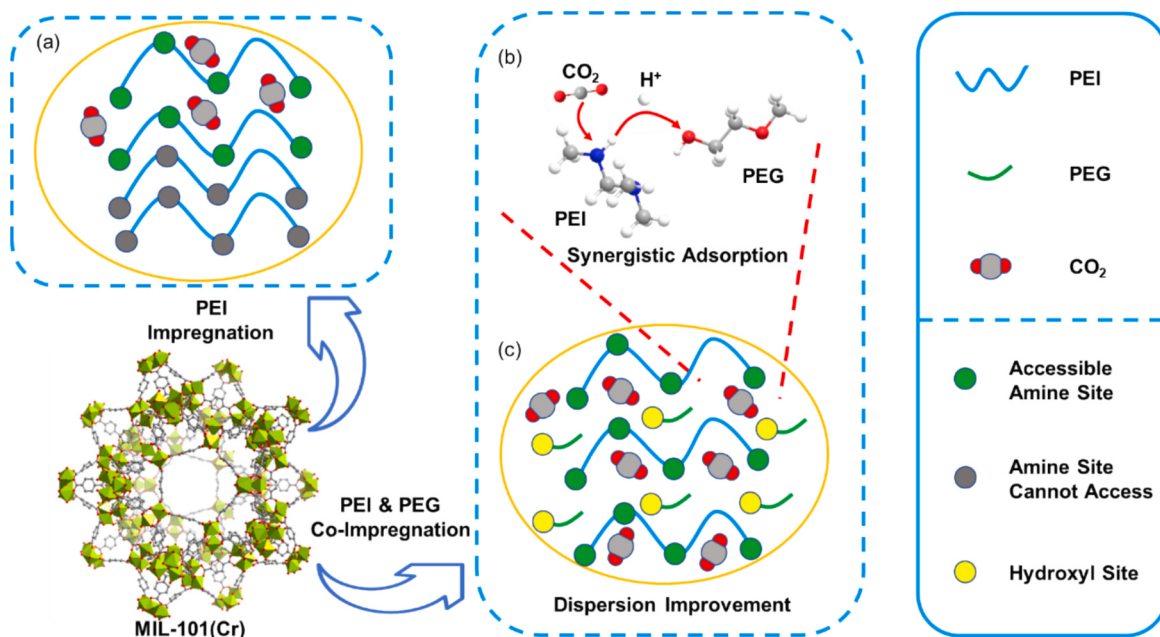


Fig. 5. The mechanism of CO₂ capture for (a) PEI-impregnated MIL-101(Cr), and (b, c) PEG/PEI co-impregnated MIL-101(Cr) based on (b) the synergistic adsorption of CO₂ with hydroxyl and amine groups, and (c) the improved dispersion of PEI.

severe aggregation, while PEG effectively improved PEI dispersion.

Therefore, the mechanism of hydroxyl-containing surfactants in improving CO₂ adsorption performance of MIL-101(Cr)-PEI is proposed. In MIL-101(Cr) loaded with PEI alone, the amine groups of PEI chemisorb CO₂, where 2 mol of amine react with 1 mol of CO₂ to form carbamate (Eq. (1)) [63]. Due to the high viscosity of PEI, its limited diffusion and uneven distribution within MIL-101(Cr) restrict the access to amine groups for CO₂ capture (Fig. 5a), resulting in lower adsorption capacity and amine efficiency than theoretical values [50,51,64].

The introduction of hydroxyl-containing surfactants such as PEG as additives serves two key functions to enhance the adsorption performance. First, the hydroxyl groups of PEG can synergistically interact with amine sites to chemically adsorb CO₂ (Eq. (2)) [52,53], promoting the formation of carbamate (Fig. 5b). Specifically, in the absence of hydroxyl groups, two amine groups are required to chemically adsorb one CO₂ molecule, with one amine group reacting with CO₂ to form carbamic acid and the other reacting with the H⁺ on the carbamic acid. In contrast, in the presence of hydroxyl groups, the hydroxyl group can neutralize the H⁺ on the carbamic acid produced by the reaction [53], which leads to the chemical adsorption of CO₂ requiring only one amino group [51,54]. Second, surfactant additives improve CO₂ adsorption by reducing the aggregation of PEI and enhancing its dispersion [53]. When PEG was present, it inserted between PEI molecules and prevented PEI aggregation, thereby enhancing CO₂ diffusion to active amine sites (Fig. 5c), which leads to higher adsorption capacity and amine efficiency.



3.4. Stability and desorption properties of CO₂ for MIL-101(Cr)-PEI with additives

To analyze the stability and desorption characteristics of the as-

synthesized composite MOFs, we selected those samples with the optimal additive concentrations (including MIL-101(Cr), MIL-101(Cr) loaded with PEI-100, PEI-100-PEG-20, PEI-100-Tween20-20, PEI-100-P123-10, PEI-100-MMEA-20, PEI-100-DEA-10, PEI-100-PPA-10, and PEI-100-DETA-10) for TGA and CO₂-TPD analysis. For the unmodified MIL-101(Cr), the TGA curve showed three distinct weight loss stages. The initial weight loss below 150 °C corresponded to solvent evaporation. The decrease between 150 and 300 °C was due to the dehydroxylation of Cr-clusters, and the weight loss between 300 and 500 °C resulted from the breakdown of the framework structure. This left a residual mass of approximately 40 % (Fig. 6a). For the MIL-101(Cr)-PEI-100, solvent loss occurred below 100 °C, likely due to the displacement of pore solvent by residual methanol during impregnation. The weight loss between 120 and 200 °C was attributed to PEI volatilization. The weight loss between 200 and 300 °C was due to the dehydroxylation of Cr-clusters [39]. The framework structure disintegrated between 300 and 500 °C, leaving a residual mass of approximately 20 %. This suggested that the addition of PEI led to an increased organic content within the structure, resulting in a lower residual mass compared to unmodified MIL-101(Cr).

For the MIL-101(Cr)-PEI-100-PEG-20 sample, the weight loss below 300 °C was lower compared to the unmodified sample. This suggested that the non-volatile surfactant interacted with PEI, reducing volatility of PEI. The residual mass decreased further to about 16 %, indicating higher incorporation amount of organic components. Samples with P123 and Tween20 additives showed similar improvements in thermal stability. In contrast, the TGA curves for samples with small molecular alkanolamine additives exhibited varied changes. DEA and DETA added to the samples resulted in increased weight loss before 300 °C, likely due to the lower boiling points of these small molecules (Fig. 6b). The MIL-101(Cr)-PEI-100-MMEA-20 and MIL-101(Cr)-PEI-100-PPA-10 showed minor reductions in weight loss in the ranges of 150–350 °C and 150–250 °C, respectively. It suggested that their interaction with PEI reduced the volatilization of PEI.

Higher desorption temperatures would result in increased energy

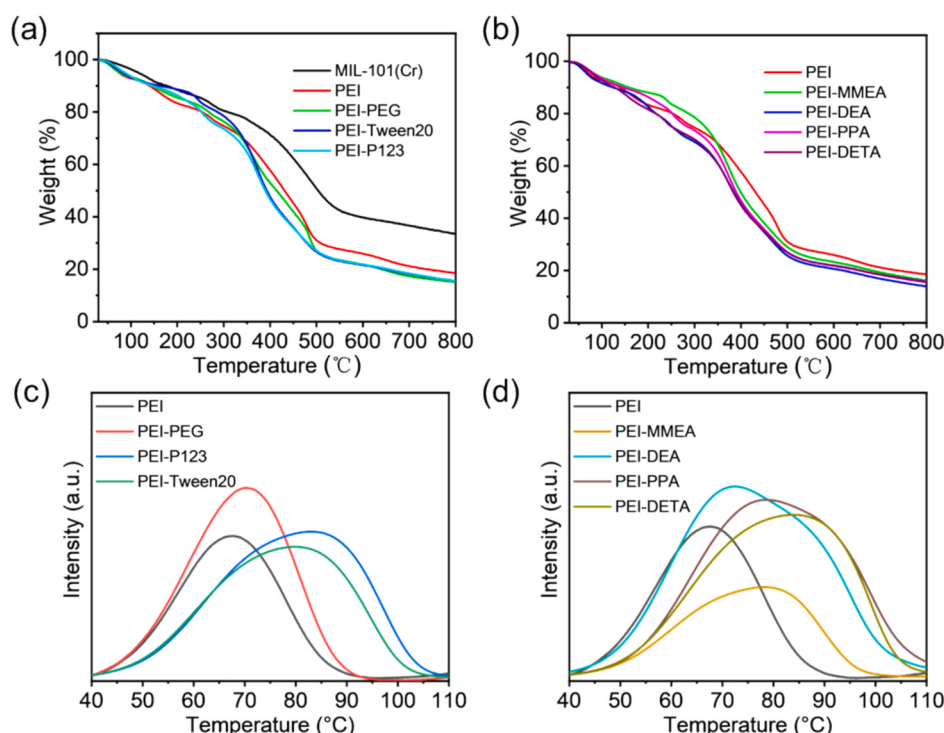


Fig. 6. TGA profiles of the as-synthesized (a) MIL-101(Cr) and MIL-101(Cr) impregnated with PEI and PEI with PEG, P123 and Tween20, and (b) MIL-101(Cr) impregnated by PEI and PEI with MMEA, DEA, PPA and DETA. The CO₂-TPD profiles of MIL-101(Cr) impregnated by PEI with (c) PEG, P123 and Tween20, and (d) MMEA, DEA, PPA and DETA.

consumption and greater equipment requirements. Moreover, at elevated temperatures, low-boiling-point small molecules are more likely to escape from MOFs substrate, potentially reducing cycling performance and undermining their practicality in DAC applications. For CO₂-TPD analysis, the desorption peak of MIL-101(Cr)-PEI-100 appears at approximately 67 °C, with complete desorption observed around 95 °C (Fig. 6c). Samples impregnated with additives displayed a shift in the desorption peak to higher temperatures, indicating that the presence of additives enhanced the interaction between the sample and CO₂. Specifically, the peak for MIL-101(Cr)-PEI-100-PEG-20 shifted to around 71 °C without altering the temperature for complete desorption. In contrast, samples impregnated with Tween 20 and P123 showed desorption peaks at approximately 80 and 85 °C, respectively, with the complete desorption temperatures increasing to around 105 and 110 °C. This shift was probably due to the larger molecular weight of the additives, which hindered the release of CO₂ molecules. Notably, samples containing small molecular amines and alcohol amines exhibited significant changes in the desorption curve, with complete desorption temperatures exceeding 110 °C and a tendency to form dual peaks (Fig. 6d). Unlike surfactant additives, alcohol amines did not improve the dispersion of PEI. Instead, the introduction of additional impregnated material within the pore cages further obstructed CO₂ desorption, leading to higher desorption temperatures. Furthermore, alcohol amines and small molecules could provide different types of amine groups compared to the amine groups of PEI, which independently reacted with CO₂ (Fig. S39) and contributed to the formation of dual peaks in CO₂-TPD. Therefore, the co-impregnating PEG and PEI in MIL-101(Cr) represents the optimal combination, achieving high adsorption capacity, amine efficiency, and lower desorption temperatures compared to other additives.

3.5. TGA CO₂ adsorption-desorption and cyclic properties of MIL-101(Cr)-PEI with additives

The adsorption kinetics results showed that MIL-101(Cr)-PEI-100 reached adsorption equilibrium after approximately 96 min (Fig. 7a). Samples incorporating PEG and Tween 20 exhibited longer equilibrium times of around 104 and 110 min, respectively, due to their higher adsorption capacities. Both samples also exhibited faster initial adsorption rates, likely owing to the improved dispersibility of PEI, which enhanced CO₂ diffusion within the MOF. In comparison, samples with P123 exhibited lower adsorption rates than those with PEG and Tween 20. This was likely due to the larger molecular size of P123, which hindered CO₂ adsorption onto active amine sites. Similarly, samples with alkanolamines and DETA also did not reach equilibrium within 120 min, indicating that these additives further slowed CO₂ adsorption (Fig. 7b). During the desorption phase, samples with PEG and Tween20 exhibited faster desorption rates and more complete desorption compared to PEI-only samples. Notably, MIL-101(Cr)-100-PEG-20 achieved complete desorption in approximately 60 min. In contrast, samples containing P123 and various alkylamines showed slower desorption rates and less complete desorption.

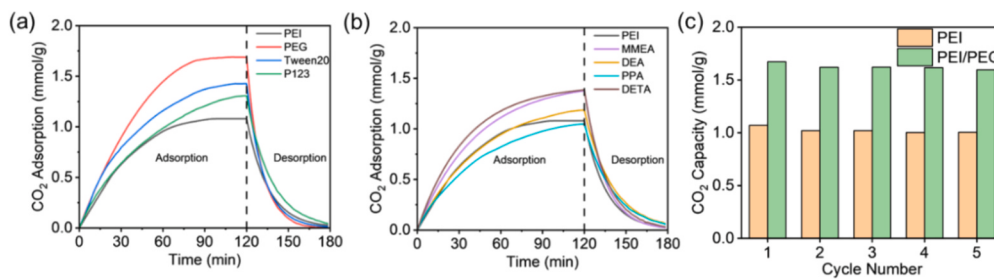


Fig. 7. TGA CO₂ adsorption and desorption profiles of MIL-101(Cr) impregnated by PEI with (a) PEG, P123 and Tween20, and (b) MMEA, DEA, PPA and DETA. (c) Cyclic CO₂ adsorption capacity column graph of MIL-101(Cr)-PEI-100 and MIL-101(Cr)-PEI-100-PEG-20.

These findings highlight the impact of additive incorporation on adsorption–desorption kinetics. Suitable additives like PEG enhance adsorption capacity and desorption efficiency by improving PEI dispersibility. In contrast, less compatible additives (such as PPA) impede CO₂ diffusion and hinder desorption, reducing overall performance.

The cyclic CO₂ adsorption capacity results showed that both MIL-101(Cr)-PEI-100 and MIL-101(Cr)-PEI-100-PEG-20 retained over 90 % of their adsorption capacity after five cycles. Specifically, MIL-101(Cr)-PEI-100-PEG-20 maintained 96 % of its initial CO₂ uptake, while MIL-101(Cr)-PEI-100 retained 94 % (Fig. 7c). This improvement was attributed to the addition of PEG, which enhanced PEI dispersibility and allowed for the regeneration of more amine sites during desorption. The cyclic CO₂ adsorption–desorption curve further showed that retained mass of MIL-101(Cr)-PEI-100 sample increased significantly after each cycle (Fig. S40). This incomplete desorption led to a decrease in cyclic capacity. In contrast, MIL-101(Cr)-PEI-100-PEG-20 exhibited lower retained mass after cycling, resulting in a higher overall cycling capacity (Fig. S41).

3.6. Breakthrough adsorption experiments

Breakthrough adsorption experiments were conducted to evaluate the performance of the functionalized materials in capturing CO₂ from flowing simulated air. The experiments were carried out in a fixed-bed reactor with a gas mixture of CO₂ and N₂ at a CO₂/N₂ volume ratio of 1:2500 and a flow rate of 300 mL/min at 25 °C. The dynamic adsorption capacity was subsequently determined using the methods described in Supporting Information S3. Fig. S42 showed the breakthrough adsorption curves for MIL-101(Cr)-PEI-100 and MIL-101(Cr)-PEI-100-PEG-20 samples. Compared to the sample impregnated with PEI alone, the addition of PEG significantly extended the complete breakthrough time from approximately 400 to 800 min. This indicated that the sample with PEG exhibited a more durable CO₂ adsorption performance when exposed to mixed gases. As shown in Fig. 8a, the cumulative CO₂ adsorption exhibited that MIL-101(Cr)-PEI-100-PEG-20 achieved a higher adsorption rate than the sample with PEI alone. The MIL-101(Cr)-PEI-100-PEG-20 sample exhibited pseudo-equilibrium adsorption capacities of 1.64 mmol/g even at a CO₂/N₂ volume ratio of 1:2500, which was comparable to the CO₂ adsorption capacity obtained using pure CO₂ gas at 400 ppm. This result demonstrated that the MIL-101(Cr)-PEI-100-PEG-20 sample not only retained a high adsorption capacity but also exhibited excellent selectivity for the chemisorption of low-concentration CO₂ in a flowing air environment.

Given the presence of moisture in ambient air, we evaluated the breakthrough adsorption performance of MIL-101(Cr)-PEI-100 and MIL-101(Cr)-PEI-100-PEG-20 under humid conditions (~100 % RH). The results showed that MIL-101(Cr)-PEI-100 and MIL-101(Cr)-PEI-100-PEG-20 samples exhibited slightly longer breakthrough and pseudo-equilibrium times under humid conditions (Fig. S43). Additionally, their adsorption capacities increased to 1.35 and 2.16 mmol/g, respectively (Fig. 8b). This enhanced adsorption performance under humid conditions can be attributed to the role of water in facilitating proton

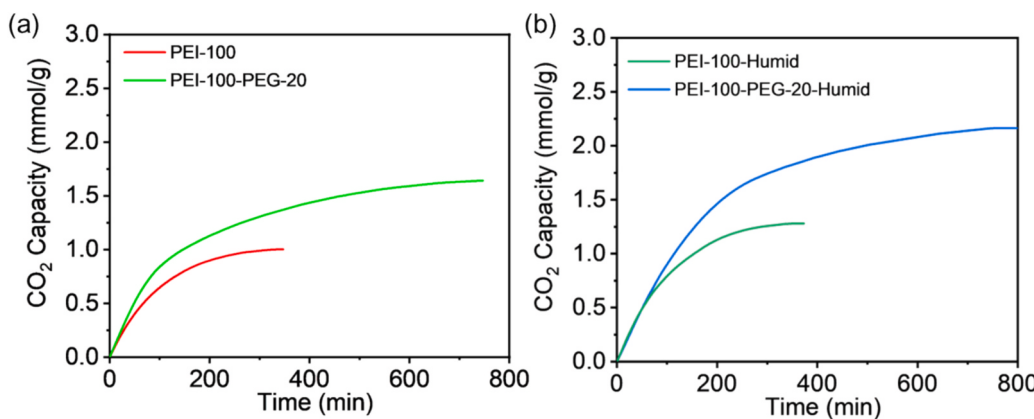


Fig. 8. Dynamic CO₂ adsorption curves of MIL-101(Cr)-PEI-100 and MIL-101(Cr)-PEI-100-PEG-20 under (a) dry, and (b) humid conditions.

transfer during the reaction between CO₂ and amines, thereby improving both the adsorption rate and capacity. Such behavior was commonly observed in PEI-impregnated and PEI/PEG co-impregnated solid amine adsorbents [65,66]. Indeed, the improvement in adsorption performance under humid conditions appeared to be independent of PEG addition, as both MIL-101(Cr)-PEI-100 and MIL-101(Cr)-PEI-100-PEG-20 samples exhibited similar adsorption capacity enhancement ratios of 34 % and 32 % compared to their performance under dry simulated air. This observation suggested that the adsorbent maintained excellent CO₂ adsorption performance under humid conditions.

4. Conclusions

In this study, we developed a green and scalable method for synthesizing MIL-101(Cr) with high specific surface area of approximately 3500 m²/g and uniform morphology, using NaOH as an additive at a relatively low reaction temperature of 130 °C. This approach avoids the use of toxic chemicals and organic solvents, making it more sustainable for large-scale production. Additionally, we investigated the impact of co-impregnation of PEI and various additives, including hydroxyl-containing surfactants, alkanolamine small molecules, and amine small molecules, into MIL-101(Cr) to enhance CO₂ adsorption. Among the tested additives, the co-impregnation of PEG and PEI proved to be the most effective, increasing the CO₂ adsorption capacity to 1.65 mmol/g and achieving an amine efficiency of around 0.159 at 25 °C and 400 ppm CO₂. This represents a significant improvement over the MIL-101(Cr)-PEI adsorbent. The improvement can be attributed to the synergistic interaction between the hydroxyl groups of PEG and the amine sites of PEI, which not only enhances CO₂ capture but also promotes better dispersion of PEI within the MIL-101(Cr) structure. Moreover, this improvement was also reflected in the adsorption kinetic performance and cyclic capacity. Under the simulated flowing air conditions (400 ppm CO₂ in N₂), the PEG and PEI co-impregnated sample demonstrated a higher adsorption capacity of 1.64 mmol/g, a faster and more sustained CO₂ removal capacity, as well as excellent selectivity. Therefore, this work presents an innovative eco-friendly synthesis method for high-performance CO₂ adsorbents, providing scalable solutions for sustainable material production and improved capture efficiency of CO₂ DAC.

Author contributions

The manuscript was written through the contributions of all authors. All authors have approved the final version of the manuscript.

CRediT authorship contribution statement

Kun Jiang: Writing – original draft, Investigation, Data curation. **Jian Yang:** Writing – review & editing, Funding acquisition. **Ximeng**

Liu: Methodology. **Yao Tong:** Investigation. **Jichang Liu:** Writing – review & editing, Funding acquisition. **Jinlou Gu:** Writing – review & editing, Conceptualization.

Declaration of competing interest

The authors declare that they have no known competing financial interests or personal relationships that could have appeared to influence the work reported in this paper.

Acknowledgments

This work was financially supported by the National Natural Science Foundation of China (52472281, 22275054, 52103314, 21975072, 51902106), Program of Shanghai Academic Research Leader (23XD1401000) and Chenguang Plan of Shanghai Education Development Foundation (21CGA38).

Appendix A. Supplementary data

Supplementary data to this article can be found online at <https://doi.org/10.1016/j.cej.2025.161643>.

Data availability

Data will be made available on request.

References

- [1] J.F. Mitchell, The “greenhouse” effect and climate change, Rev. Geophys. 27 (1) (1989) 115–139, <https://doi.org/10.1029/RG027001p00115>.
- [2] K.O. Yoro, M.O. Daramola, Chapter 1 – CO₂ emission sources, greenhouse gases, and the global warming effect, in: M.R. Rahimpour, M. Farsi, M.A. Makarem (Eds.), Advances in Carbon Capture, Woodhead Publishing, 2020, pp. 3–28, <https://doi.org/10.1016/B978-0-12-819657-1.00001-3>.
- [3] H.B. Iz, The evolution of large-scale variations in globally averaged atmospheric CO₂ concentrations since 1830, All Earth 34 (1) (2022) 16–26, <https://doi.org/10.1080/27669645.2022.2058688>.
- [4] B. Obama, The irreversible momentum of clean energy, Science 355 (6321) (2017) 126–129, <https://doi.org/10.1126/science.aam6284>.
- [5] J. Tian, L. Yu, R. Xue, S. Zhuang, Y. Shan, Global low-carbon energy transition in the post-COVID-19 era, Appl. Energy 307 (2022) 118205, <https://doi.org/10.1016/j.apenergy.2021.118205>.
- [6] D. Gielen, F. Boshell, D. Saygin, M.D. Bazilian, N. Wagner, R. Gorini, The role of renewable energy in the global energy transformation, Energy Strateg. Rev. 24 (2019) 38–50, <https://doi.org/10.1016/j.esr.2019.01.006>.
- [7] M. Bui, C.S. Adjiman, A. Bardow, E.J. Anthony, A. Boston, S. Brown, P.S. Fennell, S. Fuss, A. Galindo, L.A. Hackett, J.P. Hallett, H.J. Herzog, G. Jackson, J. Kemper, S. Krevor, G.C. Maitland, M. Matuszewski, I.S. Metcalfe, C. Petit, N. mac Dowell, Carbon capture and storage (CCS): the way forward, Energ. Environ. Sci. 11 (5) (2018) 1062–1176, <https://doi.org/10.1039/C7EE02342A>.
- [8] C. Chao, Y. Deng, R. Dewil, J. Baeyens, X. Fan, Post-combustion carbon capture, Renew. Sustain. Energ. Rev. 138 (2021) 110490, <https://doi.org/10.1016/j.rser.2020.110490>.

- [9] Y. Yang, W. Xu, Y. Wang, S.J. Hen, Y. Wang, Z. Geng, Q. Wang, T. Zhu, Progress of CCUS technology in the iron and steel industry and the suggestion of the integrated application schemes for China, *Chem. Eng. J.* 450 (2022) 138438, <https://doi.org/10.1016/j.cej.2022.138438>.
- [10] M. Erans, E.S. Sanz-Pérez, D.P. Hanak, Z. Clulow, D.M. Reiner, G.A. Mutch, Direct air capture: process technology, techno-economic and socio-political challenges, *Energ. Environ. Sci.* 15 (4) (2022) 1360–1405, <https://doi.org/10.1039/DEE03523A>.
- [11] S. Rezaei, A. Liu, P. Hovington, Emerging technologies in post-combustion carbon dioxide capture & removal, *Catal. Today* 423 (2023) 114286, <https://doi.org/10.1016/j.cattod.2023.114286>.
- [12] A. Sodiq, Y. Abdullatif, B. Aissa, A. Ostovar, N. Nassar, M. El-Naas, A. Amhammed, A review on progress made in direct air capture of CO₂, *Environ. Technol. Innov.* 29 (2023) 102991, <https://doi.org/10.1016/j.jeti.2022.102991>.
- [13] E.S. Sanz-Pérez, C.R. Murdock, S.A. Didas, C.W. Jones, Direct capture of CO₂ from ambient air, *Chem. Rev.* 116 (19) (2016) 11840–11876, <https://doi.org/10.1021/acs.chemrev.6b00173>.
- [14] J. Meckling, E. Biber, A policy roadmap for negative emissions using direct air capture, *Nat. Commun.* 12 (1) (2021) 2051, <https://doi.org/10.1038/s41467-021-22347-1>.
- [15] C.-H. Yu, C.-H. Huang, C.-S. Tan, A review of CO₂ capture by absorption and adsorption, *Aerosol Air Qual. Res.* 12 (5) (2012) 745–769, <https://doi.org/10.4209/aaqr.2012.05.0132>.
- [16] M. Yang, C. Ma, M. Xu, S. Wang, L. Xu, Recent advances in CO₂ adsorption from air: a review, *Curr. Pollut. Rep.* 5 (4) (2019) 272–293, <https://doi.org/10.1007/s40726-019-00128-1>.
- [17] A. Cherevotan, J. Raj, S.C. Peter, An overview of porous silica immobilized amines for direct air CO₂ capture, *J. Mater. Chem. A* 9 (48) (2021) 27271–27303, <https://doi.org/10.1039/DITA05961K>.
- [18] P. Zhao, G. Zhang, H. Yan, Y. Zhao, The latest development on amine functionalized solid adsorbents for post-combustion CO₂ capture: analysis review, *Chinese J. Chem. Eng.* 35 (2021) 17–43, <https://doi.org/10.1016/j.cjche.2020.11.028>.
- [19] H. Yan, J. Liu, G. Li, Y. Zhao, Y. Wang, C. Wu, W. Wu, R. Zhang, G. Zhang, Design of blend-amine solid adsorbents for CO₂ capture: enhances adsorption-equilibrium cycle strategies and mechanism, *Chem. Eng. J.* 498 (2024) 155142, <https://doi.org/10.1016/j.cej.2024.155142>.
- [20] R. Chatti, A.K. Banswal, J.A. Thote, V. Kumar, P. Jadhav, S.K. Lokhande, R. B. Biniwale, N.K. Labhsetwar, S.S. Rayalu, Amine loaded zeolites for carbon dioxide capture: amine loading and adsorption studies, *Micropor. Mesopor. Mater.* 121 (1) (2009) 84–89, <https://doi.org/10.1016/j.micromeso.2009.01.007>.
- [21] P. Zhao, Y. Yin, X. Xu, D. Yang, J. Wang, F. Yang, G. Zhang, Facile fabrication of mesoporosity silica as support for solid amine CO₂ adsorbents with enhanced adsorption capacity and kinetics, *Energy* 253 (2022) 124162, <https://doi.org/10.1016/j.energy.2022.124162>.
- [22] T.M. McDonald, W.R. Lee, J.A. Mason, B.M. Wiers, C.S. Hong, J.R. Long, Capture of carbon dioxide from air and flue gas in the alkylamine-appended metal-organic framework mmnen-Mg₂(dobpdc), *J. Am. Chem. Soc.* 134 (16) (2012) 7056–7065, <https://doi.org/10.1021/ja300034j>.
- [23] T.S. Nguyen, N.A. Dogan, H. Lim, C.T. Yavuz, Amine chemistry of porous CO₂ adsorbents, *Acc. Chem. Res.* 56 (19) (2023) 2642–2652, <https://doi.org/10.1021/acs.accounts.3c00367>.
- [24] H.K. Chae, D.Y. Siberio-Pérez, J. Kim, Y. Go, M. Eddouadi, A.J. Matzger, M. O’Keefe, O.M. Yaghi, M.D. Group, A route to high surface area, porosity and inclusion of large molecules in crystals, *Nature* 427 (6974) (2004) 523–527, <https://doi.org/10.1038/nature02311>.
- [25] Y. Lin, C. Kong, L. Chen, Amine-functionalized metal-organic frameworks: structure, synthesis and applications, *RSC Adv.* 6 (39) (2016) 32598–32614, <https://doi.org/10.1039/C6RA01536K>.
- [26] R.L. Siegelman, T.M. McDonald, M.I. Gonzalez, J.D. Martell, P.J. Milner, J. A. Mason, A.H. Berger, A.S. Bhowm, J.R. Long, Controlling cooperative CO₂ adsorption in diamine-appended Mg₂(dobpdc) metal-organic frameworks, *J. Am. Chem. Soc.* 139 (30) (2017) 10526–10538, <https://doi.org/10.1021/jacs.7b05858>.
- [27] D. Britt, H. Furukawa, B. Wang, T.G. Glover, O.M. Yaghi, Highly efficient separation of carbon dioxide by a metal-organic framework replete with open metal sites, *Proc. Natl. Acad. Sci. U.S.A.* 106 (49) (2009) 20637–20640, <https://doi.org/10.1073/pnas.0909718106>.
- [28] S. Xian, Y. Wu, J. Wu, X. Wang, J. Xiao, Enhanced dynamic CO₂ adsorption capacity and CO₂/CH₄ selectivity on polyethylenimine-impregnated UiO-66, *Ind. Eng. Chem. Res.* 54 (44) (2015) 11151–11158, <https://doi.org/10.1021/acs.iecr.5b03517>.
- [29] T.M. McDonald, J.A. Mason, X. Kong, E.D. Bloch, D. Gygi, A. Dani, V. Crocellà, F. Giordanino, S.O. Odoh, W.S. Drisdell, B. Vlaisavljevich, A.L. Dzubak, R. Poloni, S.K. Schnell, N. Planas, K. Lee, T. Pascal, L.F. Wan, R. Prendergast, J.R. Long, Cooperative insertion of CO₂ in diamine-appended metal-organic frameworks, *Nature* 519 (7543) (2015) 303–308, <https://doi.org/10.1038/nature14327>.
- [30] J. Xu, Y.M. Liu, A.S. Lipton, J. Ye, G.L. Hoatson, P.J. Milner, T.M. McDonald, R. L. Siegelman, A.C. Forse, B. Smit, J.R. Long, J.A. Reimer, Amino dynamics in diamine-appended Mg₂(dobpdc) metal-organic frameworks, *J. Phys. Chem. Lett.* 10 (22) (2019) 7044–7049, <https://doi.org/10.1021/acs.jpcllett.9b02883>.
- [31] K. Wang, Y. Li, L.H. Xie, X. Li, J.-R. Li, Construction and application of base-stable MOFs: a critical review, *Chem. Soc. Rev.* 51 (15) (2022) 6417–6441, <https://doi.org/10.1039/D1CS00891A>.
- [32] G. Férey, C. Mellot-Draznieks, C. Serre, F. Millange, J. Dutour, S. Surblé, I. Margiolaki, A chromium terephthalate-based solid with unusually large pore volumes and surface area, *Science* 309 (5743) (2005) 2040–2042, <https://doi.org/10.1126/science1116275>.
- [33] K. Munusamy, G. Sethia, D.V. Patil, P.B. Somayajulu Rallapalli, R.S. Somani, H. C. Bajaj, Sorption of carbon dioxide, methane, nitrogen and carbon monoxide on MIL-101(Cr): Volumetric measurements and dynamic adsorption studies, *Chem. Eng. J.* 195–196 (2012) 359–368, <https://doi.org/10.1016/j.cej.2012.04.071>.
- [34] L.A. Darunte, A.D. Oetomo, K.S. Walton, D.S. Sholl, C.W. Jones, Direct air capture of CO₂ using amine functionalized MIL-101(Cr), *ACS Sustain. Chem. Eng.* 4 (10) (2016) 5761–5768, <https://doi.org/10.1021/acssuschemeng.6b01692>.
- [35] G. Rim, F. Kong, M. Song, C. Rosu, P. Priyadarshini, R.P. Lively, C.W. Jones, Sub-ambient temperature direct air capture of CO₂ using amine-impregnated MIL-101(Cr) enables ambient temperature CO₂ recovery, *JACS Au* 2 (2) (2022) 380–393, <https://doi.org/10.1021/jacsau.1c00414>.
- [36] R. Zhong, X. Yu, W. Meng, J. Liu, C. Zhi, R. Zou, Amine-grafted MIL-101(Cr) via double-solvent incorporation for synergistic enhancement of CO₂ uptake and selectivity, *ACS Sustain. Chem. Eng.* 6 (12) (2018) 16493–16502, <https://doi.org/10.1021/acssuschemeng.8b03597>.
- [37] X. Huang, J. Lu, W. Wang, X. Wei, J. Ding, Experimental and computational investigation of CO₂ capture on amine grafted metal-organic framework NH₂-MIL-101, *Appl. Surf. Sci.* 371 (2016) 307–313, <https://doi.org/10.1016/j.apsusc.2016.02.154>.
- [38] J. Wang, R. Fu, S. Wen, P. Ning, M.H. Helal, M.A. Salem, B.B. Xu, Z.M. El-Bahy, M. Huang, Z. Guo, L. Huang, Q. Wang, Progress and current challenges for CO₂ capture materials from ambient air, *Adv. Compos. Hybrid Ma.* 5 (4) (2022) 2721–2759, <https://doi.org/10.1007/s42114-022-00567-3>.
- [39] L. Bromberg, Y. Diao, H. Wu, S.A. Speakman, T.A. Hatton, Chromium (III) terephthalate metal organic framework (MIL-101): HF-free synthesis, structure, polyoxometalate composites, and catalytic properties, *Chem. Mater.* 24 (9) (2012) 1664–1675, <https://doi.org/10.1021/cm2034382>.
- [40] J. Yang, Q. Zhao, J. Li, J. Dong, Synthesis of metal-organic framework MIL-101 in TMAOH-Cr (NO₃)₃-H₂BDC-H₂O and its hydrogen-storage behavior, *Micropor. Mesopor. Mater.* 130 (1) (2010) 174–179, <https://doi.org/10.1016/j.micromeso.2009.11.001>.
- [41] T. Hu, H. Lv, S. Shan, Q. Jia, H. Su, N. Tian, S. He, Porous structured MIL-101 synthesized with different mineralizers for adsorptive removal of oxytetracycline from aqueous solution, *RSC Adv.* 6 (77) (2016) 73741–73747, <https://doi.org/10.1039/C6RA11684A>.
- [42] N.A. Khan, I.J. Kang, H.Y. Seok, S.H. Jhung, Facile synthesis of nano-sized metal-organic frameworks, chromium-benzenedicarboxylate, MIL-101, *Chem. Eng. J.* 166 (3) (2011) 1152–1157, <https://doi.org/10.1016/j.cej.2010.11.098>.
- [43] U.A. Adamu, N.H.H. Abu Bakar, Z.U. Zango, N.S. Sambudi, A. Iqbal, M.H. Hussin, T.S. Hamidon, Low-temperature synthesis and characterization of porous chromium terephthalate MIL-101(Cr) and its photocatalytic degradation of phenanthrene, *Korean J. Chem. Eng.* 40 (9) (2023) 2239–2252, <https://doi.org/10.1007/s11814-023-1408-0>.
- [44] T. Zhao, F. Jeremias, I. Boldog, B. Nguyen, S.K. Henninger, C. Janiak, High-yield, fluoride-free and large-scale synthesis of MIL-101(Cr), *Dalton Trans.* 44 (38) (2015) 16791–16801, <https://doi.org/10.1039/C5DT02625C>.
- [45] A.A. Rico-Barragán, J. Raziel Álvarez, E. Hernández-Fernández, J. Rodríguez-Hernández, M.A. Garza-Navarro, N.E. Dávila-Guzmán, Green synthesis of metal-organic framework MIL-101(Cr) – an assessment by quantitative green chemistry metrics, *Polyhedron* 225 (2022) 116052, <https://doi.org/10.1016/j.poly.2022.116052>.
- [46] P.S. Ho, K.C. Chong, S.O. Lai, S.K. Mah, S.S. Lee, S.-Y. Lu, W.J. Lau, B.S. Ooi, Synthesis of MIL-101(Cr) metal organic framework by green synthesis for CO₂ gas adsorption, *IOP Conf. Ser.: Earth Environ. Sci.* 945 (1) (2021) 012074, <https://doi.org/10.1088/1755-1315/945/1/012074>.
- [47] Y. Lin, C. Kong, L. Chen, Direct synthesis of amine-functionalized MIL-101(Cr) nanoparticles and application for CO₂ capture, *RSC Adv.* 2 (16) (2012) 6417–6419, <https://doi.org/10.1039/C2RA20641B>.
- [48] G. Han, Q. Qian, K. Mizrahi Rodriguez, Z.P. Smith, Hydrothermal synthesis of sub-20 nm amine-functionalized MIL-101(Cr) nanoparticles with high surface area and enhanced CO₂ uptake, *Ind. Eng. Chem. Res.* 59 (16) (2020) 7888–7900, <https://doi.org/10.1021/acs.iecr.0c00535>.
- [49] M.Y. Zorainy, M. Gar Alalm, S. Kaliaguine, D.C. Boffito, Revisiting the MIL-101 metal-organic framework: design, synthesis, modifications, advances, and recent applications, *J. Mater. Chem. A* 9 (39) (2021) 22159–22217, <https://doi.org/10.1039/D1TA06238G>.
- [50] M.A. Sakwa-Novak, S. Tan, C.W. Jones, Role of additives in composite PEI/oxide CO₂ adsorbents: enhancement in the amine efficiency of supported PEI by PEG in CO₂ capture from simulated ambient air, *ACS Appl. Mater. Interfaces* 7 (44) (2015) 24748–24759, <https://doi.org/10.1021/acsmami.5b07545>.
- [51] Y. Wang, Y. Miao, B. Ge, Z. He, X. Zhu, S. Liu, J. Li, L. Yu, Additives enhancing supported amines performance in CO₂ capture from air, *SusMat* 3 (3) (2023) 416–430, <https://doi.org/10.1002/sus2.141>.
- [52] K. Jiang, J. Yang, Y. Zhou, J. Gu, Synergistic enhancement of CO₂ direct air capture with monoethanolamine-impregnated MIL-101(Cr) MOFs, *Micropor. Mesopor. Mater.* 366 (2024) 112920, <https://doi.org/10.1016/j.micromeso.2023.112920>.
- [53] Z. He, Y. Wang, Y. Miao, H. Wang, X. Zhu, J. Li, Mixed polyamines promote CO₂ adsorption from air, *J. Environ. Chem. Eng.* 10 (2) (2022) 107239, <https://doi.org/10.1016/j.jece.2022.107239>.
- [54] A. Arenillas, K.M. Smith, T.C. Drage, C.E. Snape, CO₂ capture using some fly ash-derived carbon materials, *Fuel* 84 (17) (2005) 2204–2210, <https://doi.org/10.1016/j.fuel.2005.04.003>.

- [55] N.A. Khan, J.W. Jun, S.H. Jhung, Effect of water concentration and acidity on the synthesis of porous chromium benzenedicarboxylates, *Eur. J. Inorg. Chem.* 2010 (7) (2010) 1043–1048, <https://doi.org/10.1002/ejic.200901064>.
- [56] W. Xu, W. Li, L. Lu, W. Zhang, J. Kang, B. Li, Morphology-control of metal-organic framework crystal for effective removal of dyes from water, *J. Solid State Chem.* 279 (2019) 120950, <https://doi.org/10.1016/j.jssc.2019.120950>.
- [57] S.H. Jhung, J.-H. Lee, J.W. Yoon, C. Serre, G. Férey, J.-S. Chang, Microwave synthesis of chromium terephthalate MIL-101 and its benzene sorption ability, *Adv. Mater.* 19 (1) (2007) 121–124, <https://doi.org/10.1002/adma.200601604>.
- [58] B. Tan, Y. Luo, X. Liang, S. Wang, X. Gao, Z. Zhang, Y. Fang, Mixed-solvothermal synthesis of MIL-101(Cr) and its water adsorption/desorption performance, *Ind. Eng. Chem. Res.* 58 (8) (2019) 2983–2990, <https://doi.org/10.1021/acs.iecr.8b05243>.
- [59] S. Mutyala, M. Jonnalagadda, H. Mitta, R. Gundeboina, CO₂ capture and adsorption kinetic study of amine-modified MIL-101 (Cr), *Chem. Eng. Res. Des.* 143 (2019) 241–248, <https://doi.org/10.1016/j.cherd.2019.01.020>.
- [60] Q. Liu, L. Ning, S. Zheng, M. Tao, Y. Shi, Y. He, Adsorption of carbon dioxide by MIL-101(Cr): regeneration conditions and influence of flue gas contaminants, *Sci. Rep.-UK* 3 (1) (2013) 2916, <https://doi.org/10.1038/srep02916>.
- [61] I. Pasquali, J.-M. Andanson, S.G. Kazarian, R. Bettini, Measurement of CO₂ sorption and PEG 1500 swelling by ATR-IR spectroscopy, *J. Supercrit. Fluid.* 45 (3) (2008) 384–390, <https://doi.org/10.1016/j.supflu.2008.01.015>.
- [62] Y. Su, J. Wang, H. Liu, FTIR spectroscopic study on effects of temperature and polymer composition on the structural properties of PEO–PPO–PEO block copolymer micelles, *Langmuir* 18 (14) (2002) 5370–5374, <https://doi.org/10.1021/la020007p>.
- [63] P. Danckwerts, The reaction of CO₂ with ethanolamines, *Chem. Eng. Sci.* 34 (4) (1979) 443–446, [https://doi.org/10.1016/0009-2509\(79\)85087-3](https://doi.org/10.1016/0009-2509(79)85087-3).
- [64] L. Zhang, X. Wang, M. Fujii, L. Yang, C. Song, CO₂ capture over molecular basket sorbents: effects of SiO₂ supports and PEG additive, *J. Energy Chem.* 26 (5) (2017) 1030–1038, <https://doi.org/10.1016/j.jec.2017.09.002>.
- [65] J. Wang, M. Wang, W. Li, W. Qiao, D. Long, L. Ling, Application of polyethylenimine-impregnated solid adsorbents for direct capture of low-concentration CO₂, *AIChE J.* 61 (3) (2015) 972–980, <https://doi.org/10.1002/aic.14679>.
- [66] S. Xian, F. Xu, C. Ma, Y. Wu, Q. Xia, H. Wang, Z. Li, Vapor-enhanced CO₂ adsorption mechanism of composite PEI@ZIF-8 modified by polyethylenimine for CO₂/N₂ separation, *Chem. Eng. J.* 280 (2015) 363–369, <https://doi.org/10.1016/j.cej.2015.06.042>.